Dynamical Conductivity and Zero-Mode Anomaly in Honeycomb Lattices

Tsuneya ANDO, Yisong ZHENG, and Hidekatsu SUZUURA

Institute for Solid State Physics, University of Tokyo
5–1–5 Kashiwanoha, Kashiwa, Chiba 277-8581

A topological anomaly present at zero energy is shown to give rise to a peculiar and singular behavior of the dynamic and static conductivity in two-dimensional honeycomb lattices. A calculation in a self-consistent Born approximation reveals that this singular dependence prevails although being somewhat smoothed out even if level broadening effects are taken into account.

§1. Introduction

Since the discovery of carbon nanotubes,[1] transport properties of the carbon network of the nanometer scale have attracted much attention. There have been a lot of experimental works focusing on the transport measurement in various nanotube structures and theoretical calculation of the conductance of carbon nanotubes.[2] A carbon nanotube consists of coaxially rolled two-dimensional graphite sheets characterized by a honeycomb lattice. Therefore, the theoretical investigation on transport properties of honeycomb lattices is instructive for the comprehensive understanding of the transport property of nanotubes. Further, a honeycomb lattice can be realized at semiconductor heterostructures with hexagonal antidot arrays.

In a previous work,[3,4] the density of states and the static magnetoconductivity were calculated by the quantum transport theory, in which short- and long-range scatterers were taken into account. It was found that the quantum theory provides conductivity exhibiting almost singular behavior in the vicinity of vanishing Fermi energy. In this paper, this behavior is shown to be a manifestation of zero-mode anomalies due to a topological singularity through the study of the dynamical conductivity.

In §2 an effective-mass scheme is reviewed briefly. In §3 the dynamical conductivity is calculated in a simplest relaxation-time approximation and it is shown that its frequency dependence is scaled by the Fermi energy and therefore becomes singular for the vanishing Fermi energy. In §4 effects of level broadening are included in a self-consistent Born approximation. It is shown that singularities prevail even in the presence of level broadening in the case of weak scattering. A summary and conclusions are given in §5.

§2. Effective-Mass Description

In a honeycomb lattice such as a two-dimensional graphite, a unit cell contains two atoms denoted as A and B as shown in Fig. 1. Two bands having approximately a linear dispersion cross the Fermi level at K and K' points of the first Brillouin zone, whose wave vectors are given by $\boldsymbol{K}=(2\pi/a)(1/3, 1/\sqrt{3})$ and $\boldsymbol{K'}=(2\pi/a)(2/3, 0)$ with a being the lattice constant. Under the half-filled condition, electronic properties are governed by states in the vicinity of K and K' points. The Schrödinger equation for such states is given by[5]

$$\mathcal{H}_0\boldsymbol{F}=\varepsilon\boldsymbol{F}, \tag{2.1}$$

with

$$\mathcal{H}_0=\begin{pmatrix} 0 & \gamma(\hat{k}_x-\mathrm{i}\hat{k}_y) & 0 & 0 \\ \gamma(\hat{k}_x+\mathrm{i}\hat{k}_y) & 0 & 0 & 0 \\ 0 & 0 & 0 & \gamma(\hat{k}_x+\mathrm{i}\hat{k}_y) \\ 0 & 0 & \gamma(\hat{k}_x-\mathrm{i}\hat{k}_y) & 0 \end{pmatrix}, \tag{2.2}$$

where γ is a band parameter, $\hat{\boldsymbol{k}}$ $(=-\mathrm{i}\vec{\nabla})$ is the wave vector operator, and $\boldsymbol{F}$ is a four-component wave function.

The eigenfunction of $\mathcal{H}_0$ is given by

$$\boldsymbol{F}^K_{s\boldsymbol{k}}(\boldsymbol{r})=\frac{1}{\sqrt{2}L}\exp(\mathrm{i}\boldsymbol{k}\cdot\boldsymbol{r})\begin{pmatrix} s \\ \mathrm{e}^{\mathrm{i}\varphi(\boldsymbol{k})} \\ 0 \\ 0 \end{pmatrix}, \tag{2.3}$$

and

$$\boldsymbol{F}^{K'}_{s\boldsymbol{k}}(\boldsymbol{r})=\frac{1}{\sqrt{2}L}\exp(\mathrm{i}\boldsymbol{k}\cdot\boldsymbol{r})\begin{pmatrix} 0 \\ 0 \\ \mathrm{e}^{\mathrm{i}\varphi(\boldsymbol{k})} \\ s \end{pmatrix}, \tag{2.4}$$

where L^2 is the area of the system, $\varphi(\boldsymbol{k})$ is the angle of the wave vector $\boldsymbol{k}$, and s denotes the bands ($s=+1$ for the conduction band and $s=-1$ for the valence band). The corresponding energy is given by

$$\varepsilon_{s\boldsymbol{k}}=s\gamma k, \tag{2.5}$$

with $k=|\boldsymbol{k}|$.

The first two components of the wave function $\boldsymbol{F}$ describe the amplitudes at a site A and B associated with the K point, and the next two those associated with the K' point. The $(4,4)$ Hamiltonian $\mathcal{H}_0$ is completely separable into $(2,2)$ components for the K and K' points in the absence of scatterers. The $(2,2)$ Hamiltonian for the K point is written as $\gamma(\vec{\sigma}\cdot\hat{\boldsymbol{k}})$ in terms of Pauli's spin matrices $\vec{\sigma}=(\sigma_x,\sigma_y)$.

We consider two different kinds of scatterers. First, the range of the scattering potential is smaller than the lattice constant of the two-dimensional graphite. When such a short-range scatterer is present at an A site $\boldsymbol{r}_i^A$, the effective Hamiltonian has been calculated as[6]

$$U_i^A(\boldsymbol{r})=\begin{pmatrix} 1 & 0 & \mathrm{e}^{\mathrm{i}\phi_i^A} & 0 \\ 0 & 0 & 0 & 0 \\ \mathrm{e}^{-\mathrm{i}\phi_i^A} & 0 & 1 & 0 \\ 0 & 0 & 0 & 0 \end{pmatrix} u_i^A\delta(\boldsymbol{r}-\boldsymbol{r}_i^A), \tag{2.6}$$

Submitted to Journal of Physical Society of Japan

with $\phi_i^A = (\boldsymbol{K}'-\boldsymbol{K})\cdot\boldsymbol{r}_i^A$ and u_i^A being the strength. Similarly, for a scatterer located at a B site $\boldsymbol{r}_i^B$,

$$U_i^B(\boldsymbol{r}) = \begin{pmatrix} 0 & 0 & 0 & 0 \\ 0 & 1 & 0 & \mathrm{e}^{\mathrm{i}\phi_i^B} \\ 0 & 0 & 0 & 0 \\ 0 & \mathrm{e}^{-\mathrm{i}\phi_i^B} & 0 & 1 \end{pmatrix} u_i^B \delta(\boldsymbol{r}-\boldsymbol{r}_i^B), \quad (2.7)$$

where $\phi_i^B = (\boldsymbol{K}'-\boldsymbol{K})\cdot\boldsymbol{r}_i^B$.

Next, the range is larger than the lattice constant but much smaller than the typical electron wavelength (which is infinite at $\varepsilon=0$). In this case matrix elements between K and K' points can be neglected and the potential is given by a diagonal matrix, i.e.,

$$U_i(\boldsymbol{r}) = \begin{pmatrix} 1 & 0 & 0 & 0 \\ 0 & 1 & 0 & 0 \\ 0 & 0 & 1 & 0 \\ 0 & 0 & 0 & 1 \end{pmatrix} u_i \delta(\boldsymbol{r}-\boldsymbol{r}_i), \quad (2.8)$$

where $\boldsymbol{r}_i$ is the impurity position. This type of scatterers is called long-range, although the potential is given by a δ function.

§3. Dynamical Conductivity

The current operator is given by

$$\boldsymbol{j} = -\frac{e\gamma}{\hbar}\vec{\sigma}, \quad (3.1)$$

for the K point. The corresponding matrix elements are calculated as

$$\begin{aligned} (s\boldsymbol{k}|j_x|s'\boldsymbol{k}') &= -\frac{e\gamma}{\hbar}\frac{1}{2}\big(s\mathrm{e}^{\mathrm{i}\varphi(\boldsymbol{k})} + s'\mathrm{e}^{-\mathrm{i}\varphi(\boldsymbol{k})}\big), \\ (s\boldsymbol{k}|j_y|s'\boldsymbol{k}') &= -\frac{e\gamma}{\hbar}\frac{-\mathrm{i}}{2}\big(s\mathrm{e}^{\mathrm{i}\varphi(\boldsymbol{k})} - s'\mathrm{e}^{-\mathrm{i}\varphi(\boldsymbol{k})}\big), \end{aligned} \quad (3.2)$$

for the K point. The dynamical conductivity is isotropic and given by

$$\sigma(\omega) = \frac{1}{L^2}\Big(\frac{e\gamma}{\hbar}\Big)^2\frac{\hbar}{\mathrm{i}} \times \sum_{ss'\boldsymbol{k}} \frac{f[\varepsilon_s(\boldsymbol{k})]-f[\varepsilon_{s'}(\boldsymbol{k})]}{[\varepsilon_s(\boldsymbol{k})-\varepsilon_{s'}(\boldsymbol{k})][\varepsilon_s(\boldsymbol{k})-\varepsilon_{s'}(\boldsymbol{k})+\hbar\omega+\mathrm{i}\delta]}, \quad (3.3)$$

where f is the Fermi distribution function, δ is a positive infinitesimal, and a factor two has been multiplied because of the presence of the K and K' points. When the Fermi energy lies in the conduction band ($\varepsilon_F=\gamma k_F \geq 0$) at zero temperature, we have

$$\sigma(\omega) = \Big(\frac{e\gamma}{\hbar}\Big)^2\frac{\hbar}{\mathrm{i}}\Big(-\frac{|\varepsilon_F|}{2\pi\gamma^2(\hbar\omega+\mathrm{i}\delta)} - \frac{1}{L^2}\sum_{|\boldsymbol{k}|>k_F}\frac{\hbar\omega+\mathrm{i}\delta}{\gamma|k|[(\hbar\omega+\mathrm{i}\delta)^2-4\gamma^2k^2]}\Big). \quad (3.4)$$

The relaxation time in the absence of a magnetic field is defined as

$$\frac{1}{\tau_0} = \frac{2\pi}{\hbar}\sum_{j'=K,K'}\sum_{s'\boldsymbol{k}'}|\langle js\boldsymbol{k}|U|j's'\boldsymbol{k}'\rangle|^2\delta(\varepsilon_{s\boldsymbol{k}}-\varepsilon_{s'\boldsymbol{k}'}), \quad (3.5)$$

where U is the effective Hamiltonian for scatterers. In the case of short-range scatterers it is given by

$$\frac{1}{\tau_0} = \frac{1}{2}\big[n_i^A\langle(u_i^A)^2\rangle + n_i^B\langle(u_i^B)^2\rangle\big]\frac{|\varepsilon|}{\hbar\gamma^2}, \quad (3.6)$$

where n_i^A and n_i^B are the concentration of scatterers in a unit area and $\langle\ldots\rangle$ means the average. The relaxation time for long-range scatterers is given by

$$\frac{1}{\tau_0} = n_i\langle(u_i)^2\rangle\frac{|\varepsilon|}{2\hbar\gamma^2}, \quad (3.7)$$

When we assume $u^2 = \langle(u_i^A)^2\rangle = \langle(u_i^B)^2\rangle = \langle(u_i)^2\rangle$ and $n_i = n_i^A + n_i^B$ and $n_i^A = n_i^B$, the relaxation time becomes same between short- and long-range cases and

$$\frac{1}{\tau_0} = \frac{2\pi|\varepsilon|}{\hbar A}, \quad (3.8)$$

where we have introduced a dimensionless parameter to characterize the scattering strength given by

$$A = \frac{4\pi\gamma^2}{n_i u^2}. \quad (3.9)$$

With the use of the Boltzmann transport equation, the transport relaxation time is given by

$$\frac{1}{\tau} = \frac{2\pi}{\hbar}\sum_{j'=K,K'}\sum_{s'\boldsymbol{k}'}|\langle js\boldsymbol{k}|U|j's'\boldsymbol{k}'\rangle|^2(1-\cos\theta)\delta(\varepsilon_{s\boldsymbol{k}}-\varepsilon_{s'\boldsymbol{k}'}), \quad (3.10)$$

where $\cos\theta = \boldsymbol{k}\cdot\boldsymbol{k}'/k^2$. We have

$$\tau(\varepsilon) = \tau_0(\varepsilon)\alpha^{-1}, \quad (3.11)$$

with $\alpha = 1$ in the case of short-range scatterers and $\alpha = 1/2$ in the case of long-range scatterers.

In order to include effects of level broadening due to scatterers, we shall replace δ by $\hbar/\tau$, where τ is a relaxation time. Because of the energy dependence of the relaxation time, we shall assume $\tau = \tau(\varepsilon)$ with $\varepsilon = \varepsilon_F$ in the first term in the right hand side of eq. (3.4) and $\varepsilon = \hbar\omega/2$ in the second term, corresponding to the energy of the states giving a major contribution to the transition. Then, the dynamical conductivity is calculated as

$$\sigma(\omega) = \frac{e^2}{8\hbar}\Big[\frac{4}{\pi}\frac{\mathrm{i}\varepsilon_F}{\hbar\omega+\mathrm{i}[\hbar/\tau(\varepsilon_F)]} + 1 + \frac{\mathrm{i}}{\pi}\ln\frac{\hbar\omega+\mathrm{i}[\hbar/\tau(\hbar\omega/2)]-2\varepsilon_F}{\hbar\omega+\mathrm{i}[\hbar/\tau(\hbar\omega/2)]+2\varepsilon_F}\Big]. \quad (3.12)$$

Because $\hbar/\tau(\varepsilon) \propto |\varepsilon|$, the frequency dependence of the dynamical conductivity is scaled by $\hbar\omega/\varepsilon_F$. Figure 2 shows $\sigma(\omega)$ as a function of $\hbar\omega/\varepsilon_F$ for several values of A.

The scaling of the dynamical conductivity $\sigma(\hbar\omega/\varepsilon_F)$ shows that $\sigma(\omega)$ exhibits a singular behavior at the point $(\omega,\varepsilon_F)=(0,0)$. In fact, when we set $\omega=0$ first, the static conductivity is given by

$$\sigma(0) = \sigma_0 \equiv \frac{e^2}{\pi^2\hbar}\frac{A}{4\alpha}, \quad (3.13)$$

independent of the Fermi energy ε_F in agreement with the Boltzmann result.[3] When we set $\varepsilon_F = 0$ first with nonzero ω, on the other hand, the static conductivity

at $\omega \to 0$ becomes $e^2/8\hbar$ which is much smaller than σ_0 in the Boltzmann limit $A \gg 1$. The correct way is to let $\omega \to 0$ at each ε_F, leading to a singular jump of the static conductivity at $\varepsilon_F = 0$. The calculation in a self-consistent Born approximation shows that this anomaly manifests itself as a near singular dependence of σ on ε_F even if level broadening effects are included and that the conductivity at $\varepsilon_F = 0$ is given by a universal conductivity quantum $e^2/\pi^2\hbar$ as will be discussed in the following.[3)]

§4. Self-Consistent Born Approximation

4.1 Green's Function

In the following we shall use Green's function technique to evaluate the dynamical conductivity.[7,8)] This technique allows us to consider broadening effects self-consistently and is widely used. The Green's function (resolvent) is defined by

$$G(\varepsilon) = \frac{1}{\varepsilon - \mathcal{H}}. \tag{4.1}$$

The matrix elements of unperturbed Green's function are diagonal:

$$G^{(0)}_{\mu\mu'}(\varepsilon) = \Big(\mu\Big|\frac{1}{\varepsilon-\mathcal{H}_0}\Big|\mu\Big) = \frac{\delta_{\mu\mu'}}{\varepsilon-\varepsilon_\mu} \equiv \delta_{\mu\mu'}G^{(0)}_\mu(\varepsilon), \tag{4.2}$$

where $\mu = (j, s, \boldsymbol{k})$ with $j = K$ or K' and $s = \pm 1$. For evaluating physical quantities, we need $\langle G_{\mu\mu'}(\varepsilon)\rangle$, which is the average of the matrix element of $G(\varepsilon)$ over all possible configuration of random distributions of impurities. The averaged Green's function is connected to the proper self-energy $\Sigma_{\mu\mu'}(\varepsilon)$ by Dyson's equation:

$$\langle G_{\mu\mu'}(\varepsilon)\rangle = \delta_{\mu\mu'}G^{(0)}_\mu(\varepsilon) + G^{(0)}_\mu(\varepsilon)\sum_{\mu''}\Sigma_{\mu\mu''}(\varepsilon)\langle G_{\mu''\mu'}(\varepsilon)\rangle. \tag{4.3}$$

Figure 3 shows a diagramatic representation of the self-consistent Born approximation. The self-energy is given by

$$\Sigma_{\mu\mu'}(\varepsilon) = \sum_{\mu_1\mu_1'}\langle U_{\mu\mu_1}U_{\mu_1'\mu'}\rangle\langle G_{\mu_1\mu_1'}(\varepsilon)\rangle, \tag{4.4}$$

where terms lowest-order in U are neglected because they can be absorbed into a shift in the energy origin. For the choice of the scattering parameters discussed in the previous section, the self-energy and Green's function become independent of short- and long-range scatterers. We have

$$\begin{aligned}\Sigma_{\mu\mu'}(\varepsilon) &= \delta_{\mu\mu'}\Sigma(\varepsilon),\\ \langle G_{\mu\mu'}(\varepsilon)\rangle &= \delta_{\mu\mu'}G_\mu(\varepsilon),\end{aligned} \tag{4.5}$$

with

$$\Sigma(\varepsilon) = \frac{n_{\rm i}u^2}{4L^2}\sum_\mu G_\mu(\varepsilon), \tag{4.6}$$

and

$$G_\mu(\varepsilon) = \frac{1}{\varepsilon - \varepsilon_\mu - \Sigma(\varepsilon)}. \tag{4.7}$$

Explicitly, we have

$$\Sigma(\varepsilon) = \frac{n_{\rm i}u^2}{2\pi}[\varepsilon - \Sigma(\varepsilon)]\int_0^{k_c}\frac{k{\rm d}k}{[\varepsilon-\Sigma(\varepsilon)]^2 - \gamma^2k^2}, \tag{4.8}$$

where k_c is a cutoff wave number. Define

$$X(\varepsilon) = \varepsilon - \Sigma(\varepsilon). \tag{4.9}$$

Then, the self-consistency equation is rewritten as

$$\varepsilon = X(\varepsilon) + \frac{1}{A}X(\varepsilon)\big(\ln X(\varepsilon)^2 - \ln[X(\varepsilon)^2 - \varepsilon_c^2]\big), \tag{4.10}$$

where

$$\varepsilon_c = \gamma k_c. \tag{4.11}$$

The cutoff k_c is given by $k_c \sim 2\pi/a$ where a is the lattice constant and the corresponding ε_c is of the order of the band width.[9,10)]

The Boltzmann result for scattering rate can be obtained by taking the limit $X(\varepsilon) = X_0'(\varepsilon) \equiv \varepsilon + {\rm i}0$ in the second term of the right hand side of eq. (4.10) as

$$X''(\varepsilon+{\rm i}0) \equiv X_0''(\varepsilon+{\rm i}0) = {\rm i}\frac{\pi}{A}|\varepsilon| = {\rm i}\frac{\hbar}{2\tau_0(\varepsilon)}, \tag{4.12}$$

with $X'(\varepsilon+{\rm i}0) = {\rm Re}X(\varepsilon+{\rm i}0)$ and $X''(\varepsilon+{\rm i}0) = {\rm Im}X(\varepsilon+{\rm i}0)$. This lowest order result is valid in the case of weak scattering $A \gg 1$ and $\varepsilon \neq 0$.

The density of states is given by

$$D(\varepsilon) = -\frac{1}{\pi L^2}\sum_\mu {\rm Im}\langle G_{\mu\mu}(\varepsilon+{\rm i}0)\rangle = \frac{4{\rm Im}X(\varepsilon+{\rm i}0)}{\pi n_{\rm i}u^2}, \tag{4.13}$$

which gives that in the absence of impurities upon substitution of $X_0(\varepsilon+{\rm i}0) = X_0'(\varepsilon+{\rm i}0) + {\rm i}X_0''(\varepsilon+{\rm i}0)$,

$$D_0(\varepsilon) = \frac{|\varepsilon|}{\pi\gamma^2}. \tag{4.14}$$

4.2 Dynamical Conductivity

The conductivity is written as

$$\begin{aligned}\sigma_{xx}(\omega) = -\frac{2\hbar}{4\pi L^2}\int{\rm d}\varepsilon\frac{f(\varepsilon)-f(\varepsilon+\hbar\omega)}{\hbar\omega}\sum_\pm(\pm)\sum_\pm(\pm)\sum_{ss'\boldsymbol{k}}\\ \times (s'\boldsymbol{k}|j_x|s\boldsymbol{k})G_{s\boldsymbol{k}}(\varepsilon+\hbar\omega\pm{\rm i}0)G_{s'\boldsymbol{k}}(\varepsilon\pm{\rm i}0)\\ \times J_x^{ss'\boldsymbol{k}}(\varepsilon+\hbar\omega\pm{\rm i}0, \varepsilon\pm{\rm i}0),\end{aligned} \tag{4.15}$$

where $J_x^{ss'\boldsymbol{k}}(\varepsilon+\hbar\omega\pm{\rm i}0, \varepsilon\pm{\rm i}0)$ is the current vertex part as shown in Fig. 3 and the factor two is due to the presence of the K and K' points. In the case of short-range scatterers, vertex corrections vanish identically and we have

$$J_x^{ss'\boldsymbol{k}}(\varepsilon, \varepsilon') = (s\boldsymbol{k}|j_x|s'\boldsymbol{k}). \tag{4.16}$$

In the case of long-range scatterers, we have

$$J_x^{ss'\boldsymbol{k}}(\varepsilon, \varepsilon') = (s\boldsymbol{k}|j_x|s'\boldsymbol{k})\big[1 - A^{-1}\phi(\varepsilon, \varepsilon')\big]^{-1}, \tag{4.17}$$

with

$$\phi(\varepsilon, \varepsilon') = \frac{\pi\gamma^2}{L^2}\sum_{ss'\boldsymbol{k}}G_{s\boldsymbol{k}}(\varepsilon)G_{s'\boldsymbol{k}}(\varepsilon'). \tag{4.18}$$

Explicitly, we have

$$\phi(\varepsilon,\varepsilon') = \frac{X(\varepsilon)X(\varepsilon')}{X(\varepsilon')^2-X(\varepsilon)^2}\big(\ln X(\varepsilon)^2-\ln X(\varepsilon')^2 -\ln[X(\varepsilon)^2-\varepsilon_c^2]+\ln[X(\varepsilon')^2-\varepsilon_c^2]\big). \tag{4.19}$$

When $\varepsilon'=\varepsilon$ we have

$$\begin{aligned}\phi(\varepsilon+\mathrm{i}0,\varepsilon+\mathrm{i}0) &= -1,\\ \phi(\varepsilon+\mathrm{i}0,\varepsilon-\mathrm{i}0) &= S(\varepsilon),\end{aligned} \tag{4.20}$$

with

$$S(\varepsilon) = \frac{|X(\varepsilon+\mathrm{i}0)|^2}{X'(\varepsilon+\mathrm{i}0)X''(\varepsilon+\mathrm{i}0)}\tan^{-1}\frac{X'(\varepsilon+\mathrm{i}0)}{X''(\varepsilon+\mathrm{i}0)}. \tag{4.21}$$

Therefore, the dynamical conductivity is given by

$$\sigma(\omega) = -\frac{e^2}{4\pi^2\hbar}\int \mathrm{d}\varepsilon \frac{f(\varepsilon)-f(\varepsilon+\hbar\omega)}{\hbar\omega}\sum_{\pm}(\pm)\sum_{\pm}(\pm) \times \phi(\varepsilon+\hbar\omega\pm\mathrm{i}0,\varepsilon\pm\mathrm{i}0)\Xi(\varepsilon+\hbar\omega\pm\mathrm{i}0,\varepsilon\pm\mathrm{i}0), \tag{4.22}$$

with

$$\Xi(\varepsilon+\hbar\omega\pm\mathrm{i}0,\varepsilon\pm\mathrm{i}0) = 1, \tag{4.23}$$

for short-range scatterers and

$$\Xi(\varepsilon+\hbar\omega\pm\mathrm{i}0,\varepsilon\pm\mathrm{i}0) = \big[1-A^{-1}\phi(\varepsilon+\hbar\omega\pm\mathrm{i}0,\varepsilon\pm\mathrm{i}0)\big]^{-1}, \tag{4.24}$$

for long-range scatterers.

The above results give the static conductivity calculated previously[3] in the limit $\omega\to 0$. In fact, in the case of short-range scatterers, the static conductivity becomes

$$\sigma = \frac{1}{2}\frac{e^2}{\pi^2\hbar}\big[S(\varepsilon_F)+1\big], \tag{4.25}$$

at zero temperature. In the Boltzmann limit $A\gg 1$, we have $|\varepsilon_F|/X''(\varepsilon_F+\mathrm{i}0)\gg 1$ and therefore $\sigma=\sigma_0$ given by eq. (3.13) with $\alpha=1$. In the particular case $\varepsilon=0$, the real part of the self-energy vanishes at $\varepsilon=0$ because of the symmetry between $\varepsilon>0$ and $\varepsilon<0$ and eq. (4.10) gives immediately $X(+\mathrm{i}0)=\mathrm{i}\varepsilon_c\exp(-A/2)$. The conductivity at $\varepsilon_F=0$ is also calculated analytically and becomes

$$\sigma = \frac{e^2}{\pi^2\hbar}. \tag{4.26}$$

This conductivity is given only by natural constants and independent of the scattering strength and the band parameter. Further, it is much smaller than the Boltzmann conductivity σ_0 in the case of weak scattering $A\gg 1$.

In the case of long-range scatterers, on the other hand, we have

$$\sigma = \frac{e^2}{\pi^2\hbar}\frac{S(\varepsilon_F)+1}{(1+A^{-1})[1-A^{-1}S(\varepsilon_F)]}. \tag{4.27}$$

In the Boltzmann limit, we have $S(\varepsilon_F)=A/2$ and $\sigma=\sigma_0$ with $\alpha=1/2$. Further, at $\varepsilon_F=0$, we have $S(\varepsilon_F)=1$ and therefore

$$\sigma = \frac{e^2}{\pi^2\hbar}\frac{1}{1-A^{-2}} \approx \frac{e^2}{\pi^2\hbar}. \tag{4.28}$$

This value is slightly larger than $e^2/\pi^2\hbar$ and dependent on the scattering parameter. This dependence is extremely small in the case of weak scattering $A\gg 1$.

§5. Numerical Results

The important energy scale in the present problem is the cutoff energy ε_c which is of the order of the band width. However, in this paper, following ref. 3, we shall introduce an arbitrary energy scale ε_0 which is assumed to have the same order of magnitude as other relevant energies such as ε and $X(\varepsilon+\mathrm{i}0)$ and choose the cutoff energy as $\varepsilon_c/\varepsilon_0=50$.

Figure 4 shows some examples of calculated $\sigma(\omega)$ for different values of ε_F and for $A=50$ and 20 in the case of short-range scatterers. The frequency dependence is scaled by $\hbar\omega/\varepsilon_F$ as long as $\varepsilon_F\neq 0$ for weaker scattering $A=50$. When ε_F is very close to 0, however, the conductivity at $\omega=0$ becomes small and the discrete jump present in the Boltzmann conductivity is removed as is more clear in the case of stronger scattering $A=20$. The energy scale causing this crossover behavior becomes smaller with A leading to a singular behavior of the dynamical conductivity in the weak scattering limit.

Figure 5 shows some examples in the case of long-range scatterers. The behavior is essentially same as in the case of short-range scatterers except that effects of scattering are reduced. This reduction corresponds to the increase of the transport relaxation time due to the absence of backward scattering.[3,6,11]

§6. Discussion

The anomalous behaviors of the static and dynamic conductivities at $\varepsilon_F=0$ are closely related to the zero-mode anomaly due to a topological singularity at $\boldsymbol{k}=0$ present in Weyl's equation describing the electronic states near the K and K' points. In fact, when $\boldsymbol{k}$ is rotated once in the anticlockwise direction adiabatically as a function of time t for a time interval $0<t<T$ with $\boldsymbol{k}(T)=\boldsymbol{k}(0)$, the wavefunction $\boldsymbol{F}_{s\boldsymbol{k}}$ is changed into $\boldsymbol{F}_{s\boldsymbol{k}}\exp(-\mathrm{i}\varphi)$, where φ is Berry's phase given by[12,11]

$$\varphi = -\mathrm{i}\int_0^T \mathrm{d}t\,\Big\langle s\boldsymbol{k}(t)\Big|\frac{\mathrm{d}}{\mathrm{d}t}\Big|s\boldsymbol{k}(t)\Big\rangle = -\pi. \tag{6.1}$$

It should be noted that $\varphi=-\pi$ when the closed contour encircles the origin $\boldsymbol{k}=0$ but $\varphi=0$ when the contour does not contain $\boldsymbol{k}=0$. Further, the wave function at $\boldsymbol{k}=0$ depends on the direction of $\boldsymbol{k}$ even if it is undefined at $\boldsymbol{k}=0$. These facts show the presence of a topological singularity at $\boldsymbol{k}=0$.

This nontrivial Berry's phase leads to the unique property of a metallic carbon nanotube that there exists no backward scattering and the tube is a perfect conductor even in the presence of scatterers as long as their potential range is larger than the lattice constant.[6,11]

This Berry's phase is closely related to the helicity of a neutrino and the signature change of a wave function under a spin rotation. In fact, the Schrödinger equation near the K point is written as

$$\gamma(\vec{\sigma}\cdot\hat{\boldsymbol{k}})\boldsymbol{F}^K = \varepsilon\boldsymbol{F}^K, \tag{6.2}$$

using the spin matrix $\vec{\sigma}$. This shows clearly that the spin

is quantized into the direction of $\boldsymbol{k}$ and the wave function is given by a spinor with its spin in the $\boldsymbol{k}$ direction. The spin function changes its signature when the spin is rotated by 2π. This well-known signature change under the spin rotation corresponds to the above Berry's phase.

A singularity at $\varepsilon = 0$ manifests itself in magnetic fields even in classical mechanics. The equation of motion is given by

$$\hbar \frac{d\boldsymbol{k}}{dt} = -\frac{e}{c}\boldsymbol{v} \times \boldsymbol{B}. \tag{6.3}$$

This gives the cyclotron frequency $\omega_c = eBv^2/c\varepsilon$, where v is the electron velocity given by $v = |\boldsymbol{v}| = \gamma/\hbar$. The cyclotron frequency ω_c diverges and changes its signature at $\varepsilon = 0$.[4)]

In quantum mechanics $\hat{k}_x$ and $\hat{k}_y$ satisfy the commutation relation $[\hat{k}_x, \hat{k}_y] = -\mathrm{i}/l^2$, where l is the magnetic length given by $l = \sqrt{c\hbar/eB}$. Semiclassically, the Landau levels can be obtained by the condition

$$\oint k_x dk_y = \frac{2\pi}{l^2}(n+\delta), \tag{6.4}$$

with integer n and an appropriate small correction δ. This gives $\varepsilon_n = \pm\sqrt{n+\delta}\,(\sqrt{2}\gamma/l)$. Because of the uncertainty relation $\Delta k_x \Delta k_y \sim l^{-2}$, $k^2 = 0$ is not allowed and there is no Landau level at $\varepsilon = 0$. However, a full quantum mechanical treatment of a magnetic field leads immediately to the formation of Landau levels at $\varepsilon_n = \mathrm{sgn}(n)(\sqrt{2}\gamma/l)\sqrt{|n|}$ with $n = 0, \pm 1, \pm 2, \ldots$. A peculiar and intriguing feature is the presence of a Landau level at $\varepsilon = 0$. This is presumably related also to the anomaly present at $\varepsilon = 0$.

In the Boltzmann transport theory the conductivity tensor $\sigma_{\mu\nu}$ with $\mu = x, y$ and $\nu = x, y$ is given by

$$\begin{aligned} \sigma_{xx} &= \sigma_{yy} = \frac{\sigma_0}{1+(\omega_c\tau)^2}, \\ \sigma_{xy} &= -\sigma_{yx} = -\frac{\sigma_0\omega_c\tau}{1+(\omega_c\tau)^2}, \end{aligned} \tag{6.5}$$

where σ_0 is defined in eq. (3.13). Using the explicit expressions for ω_c and τ, we have

$$\begin{aligned} \sigma_{xx} &= \sigma_0 \frac{\xi^4}{1+\xi^4}, \\ \sigma_{xy} &= -\sigma_0 \frac{\xi^2}{1+\xi^4}, \end{aligned} \tag{6.6}$$

with

$$\xi = \sqrt{\frac{2\pi\alpha}{A}}\frac{\varepsilon_F}{\varepsilon_B}, \tag{6.7}$$

where ε_B is the magnetic energy defined by $\varepsilon_B = \gamma/l$. Because the dependence on the Fermi energy is fully scaled by ε_B, the conductivities exhibit a singular behavior at $\varepsilon_F = 0$ in the limit of the vanishing magnetic field $\varepsilon_B \to 0$.

This singularity at $\varepsilon_F = 0$ disappears in the quantum theory based on the self-consistent Born approximation. Figure 6 compares classical and quantum σ_{xx} and σ_{xy} as a function of ξ for $A = 50$ in the case of short-range scatterers and Fig. 7 shows corresponding comparison in the case of long-range scatterers. In contrast to the Boltzmann result the quantum results depend on $\varepsilon_B/\varepsilon_0$ and σ_{xx} depends on the Fermi energy in the limit $\varepsilon_B/\varepsilon_0 \to 0$, in consistent with previous results.[3,4)]

§7. Summary

In summary, we have discussed anomalies appearing in the static and dynamic conductivity associated with the topological singularity at $\boldsymbol{k} = 0$. In the Boltzmann transport theory, the frequency dependence of the dynamical conductivity is determined by $\hbar\omega/\varepsilon_F$ leading to a singular jump at $\omega = 0$ and $\varepsilon_F = 0$. Therefore, the static conductivity has a singularity at $(\omega, \varepsilon_F) = (0, 0)$ and depends critically on which of ω and ε_F is set equal to zero first. In a self-consistent Born approximation in which level broadening effects are properly taken into account, this singular dependence is somewhat smoothed out but the corresponding energy scale is determined by the broadening at $\varepsilon_F \approx 0$ and is extremely small in the case of weak scattering.

Acknowledgments

This work was supported in part by Grants-in-Aid for Scientific Research and for COE (12CE2004 "Control of Electrons by Quantum Dot Structures and Its Application to Advanced Electronics") from Ministry of Education, Culture, Sports, Science and Technology Japan. Numerical calculations were performed in part using the facilities of the Supercomputer Center, Institute for Solid State Physics, University of Tokyo.

References

1) S. Iijima: Nature (London) **354** (1991) 56.
2) See, for example, T. Ando: Semicond. Sci. Technol. **15** (2000) R13 and references cited therein.
3) N. H. Shon and T. Ando: J. Phys. Soc. Jpn. **67** (1998) 2421.
4) Y. Zheng and T. Ando: Phys. Rev. B (submitted for publication).
5) J. C. Slonczewski and P. R. Weiss: Phys. Rev. **109** (1958) 272.
6) T. Ando and T. Nakanishi: J. Phys. Soc. Jpn. **67** (1998) 1704.
7) T. Ando and Y. Uemura: J. Phys. Soc. Jpn. **36** (1974) 959.
8) T. Ando: J. Phys. Soc. Jpn. **36** (1974) 1521; **37** (1974) 622; **37** (1974) 1233.
9) T. Ando, T. Nakanishi, and M. Igami: J. Phys. Soc. Jpn. **68** (1999) 3994.
10) H. Matsumura and T. Ando: J. Phys. Soc. Jpn. **70** (2001) 2657.
11) T. Ando, T. Nakanishi, and R. Saito: J. Phys. Soc. Jpn. **67** (1998) 2857.
12) M. V. Berry: Proc. Roy. Soc. London **A392** (1984) 45.

Figure Captions

Fig. 1 The structure of a honeycomb lattice and its first Brillouin zone. A unit cell contains two atoms denoted as A and B (small circles). The corner points of the Brillouin zone are denoted as K and K'. A honeycomb lattice can be realized at a semiconductor heterostructure by fabrication of a

short-period hexagonal antidot array (shadowed big circles).

Fig. 2 The dynamical conductivity calculated using the Boltzmann transport equation. The frequency is scaled by the Fermi energy. $\alpha = 1$ and $1/2$ in the case of short- and long-range scatterers, respectively.

Fig. 3 Some diagrams in the self-consistent Born approximation. The top shows the diagram of the self-energy for intravalley scattering processes and for intervalley. The middle shows the diagram of the conductivity with vertex corrections. The bottom shows the equation for the current vertex part.

Fig. 4 Some examples of calculated dynamical conductivity in the case of short-range scatterers. (a) $A = 50$. (b) $A = 20$.

Fig. 5 Some examples of calculated dynamical conductivity in the case of long-range scatterers. (a) $A = 50$. (b) $A = 20$.

Fig. 6 The diagonal σ_{xx} and Hall σ_{xy} conductivity as a function of the normalized Fermi energy in the case of short-range scatterers. The thick lines represent Boltzmann results and the thin lines those obtained in the self-consistent Born approximation.

Fig. 7 The diagonal σ_{xx} and Hall σ_{xy} conductivity as a function of the normalized Fermi energy in the case of long-range scatterers. The thick lines represent Boltzmann results and the thin lines those obtained in the self-consistent Born approximation.

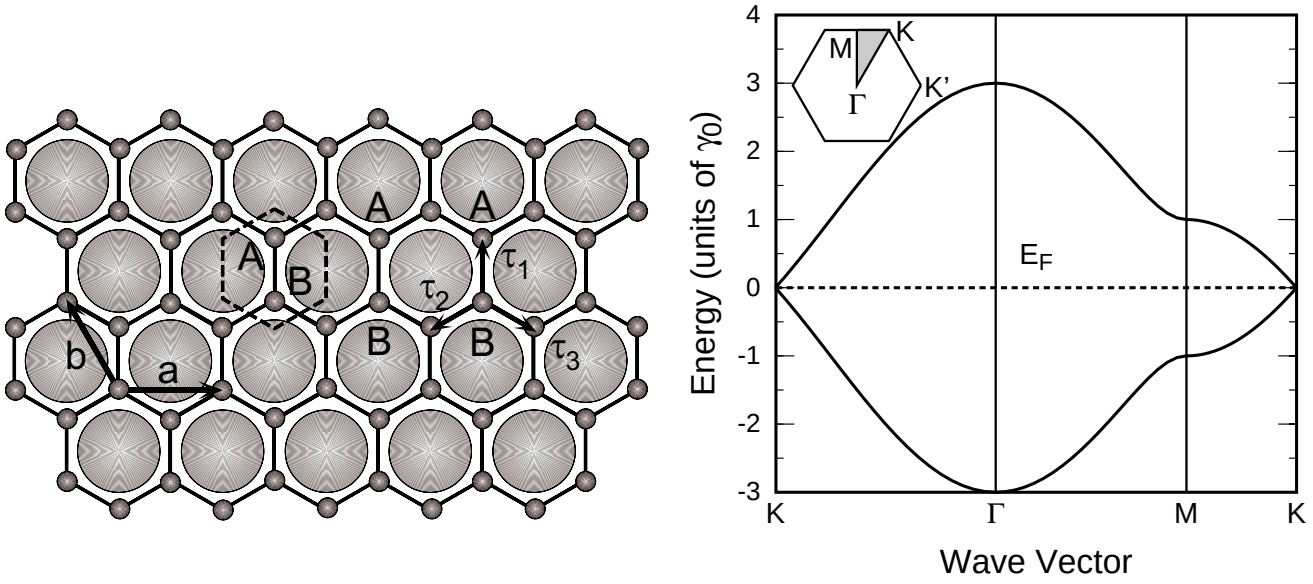

Fig. 1

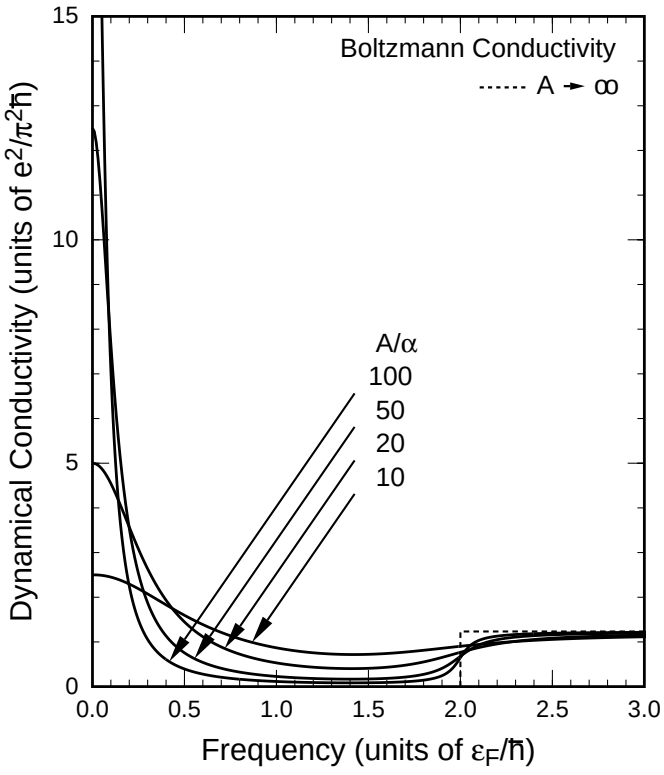

Fig. 2

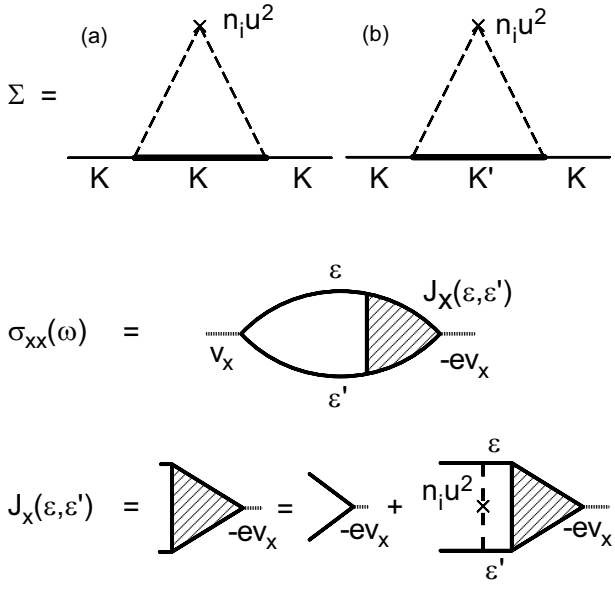

Fig. 3

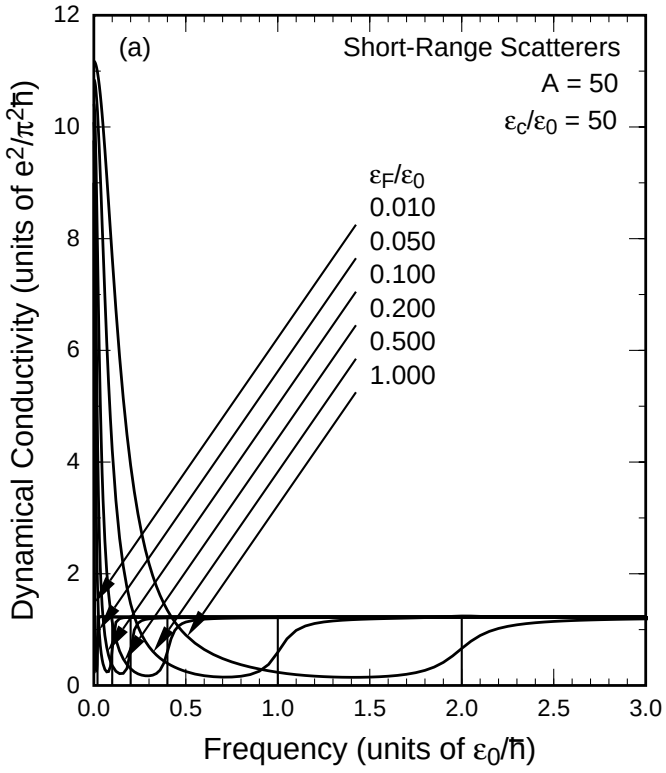

Fig. 4(a)

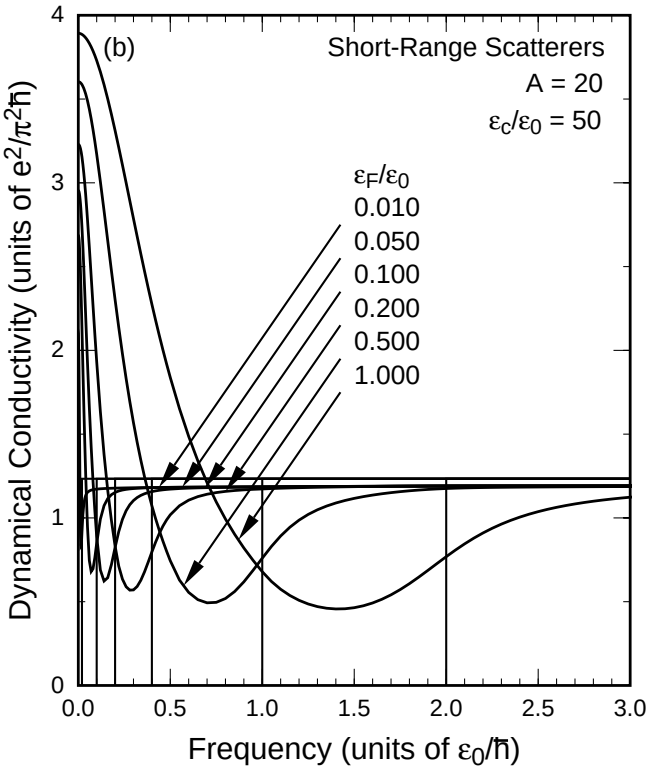

Fig. 4(b)

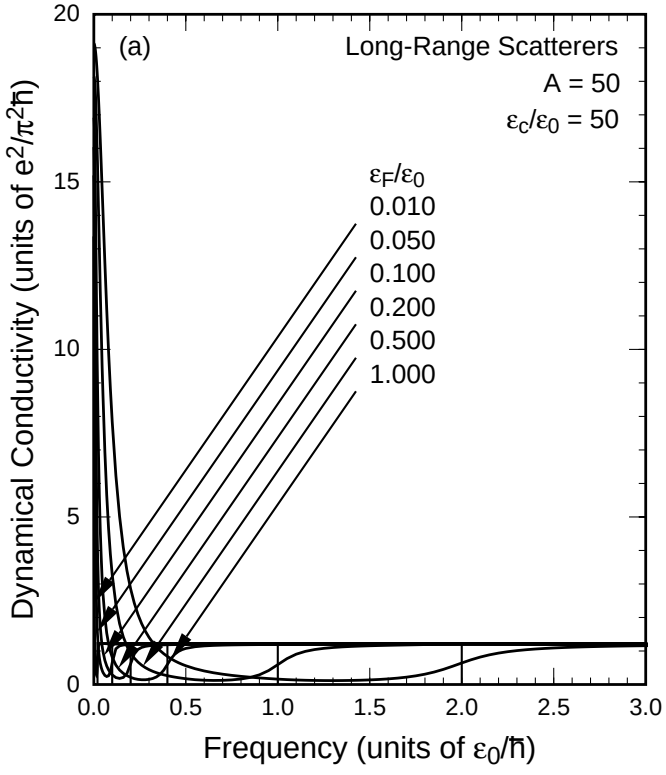

Fig. 5(a)

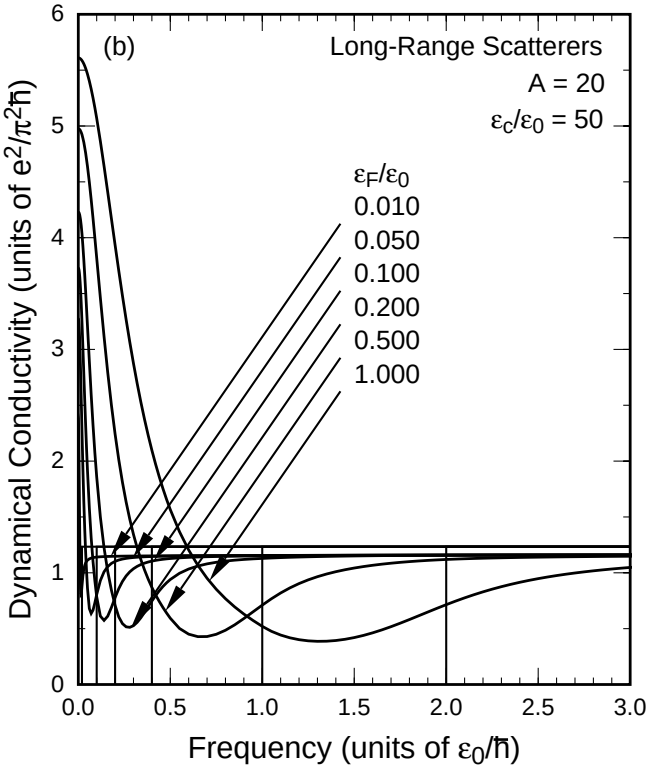

Fig. 5(b)

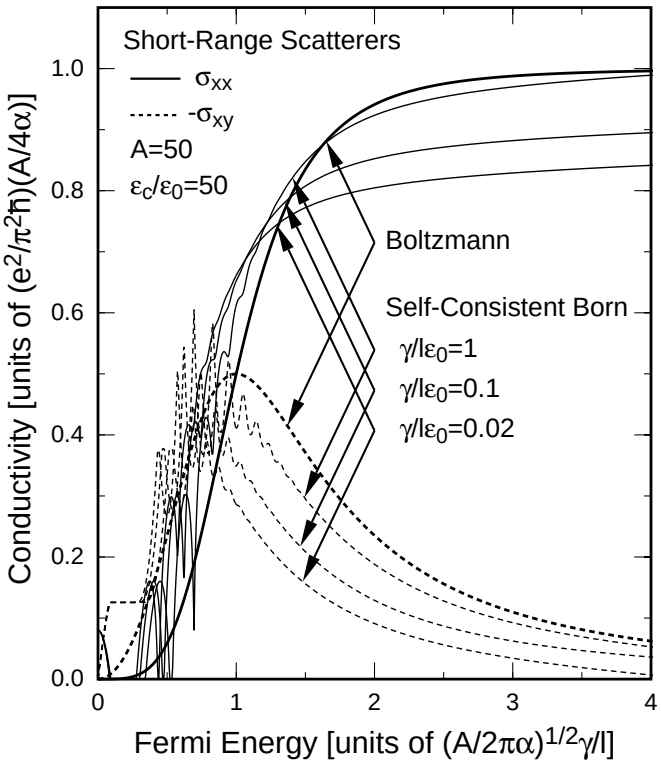
Short-Range Scatterers
σxx
-σxy
A=50
εc/ε0=50
Boltzmann
Self-Consistent Born
γ/lε0=1
γ/lε0=0.1
γ/lε0=0.02
Conductivity [units of (e2/π2ħ)(A/4α)]
Fermi Energy [units of (A/2πα)1/2γ/l]
0.0
0.2
0.4
0.6
0.8
1.0
0
1
2
3
4

Fig. 6

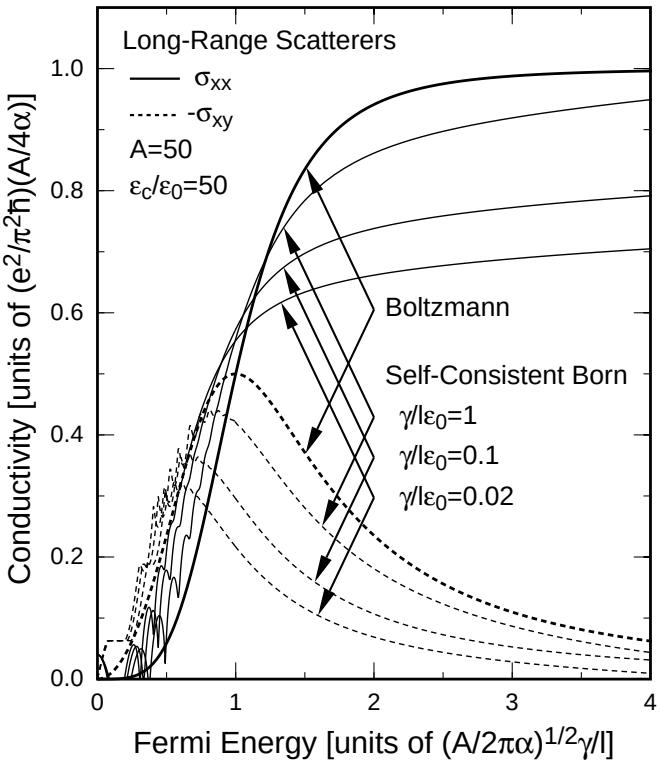
Long-Range Scatterers
σxx
-σxy
A=50
εc/ε0=50
Boltzmann
Self-Consistent Born
γ/lε0=1
γ/lε0=0.1
γ/lε0=0.02
Conductivity [units of (e2/π2ħ)(A/4α)]
Fermi Energy [units of (A/2πα)1/2γ/l]
0.0
0.2
0.4
0.6
0.8
1.0
0
1
2
3
4

Fig. 7